OXFORD JOURNAL
OF STUDENT
SCHOLARSHIP

Design, Fabrication, and Experimental Performance Analysis of a Prototype Archimedes Spiral Wind Turbine

Aryaman Nijhawan
nijhawanaryaman@gmail.com

ABSTRACT

SpiralWatt was an experimental 3D-printed Archimedes spiral wind turbine that had as its purpose to determine if a rotor in conjunction with solar cells would be able to generate enough electricity to operate LEDs. Four three-blade PLA rotors ranging in size from 5–14 cm radius and weighing 30–200 grams were attached to a single DC generator which operated at a fixed 29.2-ohm resistive load. Test results indicated that the four rotors generated between 3.6 mW and 70.4 mW. Results also indicated that the smallest rotor produced the most electrical energy (70.4 ± 2.7 mW) at 12.3 m/s. It was determined that the reason for the larger rotors generating less electrical energy than expected was primarily because of their lower rotational speed and improper matching with the DC generator. The tip-speed ratio remained relatively stable with changing wind speed for each rotor, with values around 1.15 for Sample 1 and 1.5–1.7 for Samples 2–4, but the uncertainty associated with the measurements taken during testing was between 27% and 45%. Because mass and blade geometry were varied along with the rotor size it is impossible to draw conclusions about how changes in rotor size alone affect turbine performance. When the solar cells powered the LED, the maximum directly measured voltage generated by the wind turbine (1.52 V) was not high enough to supplement the solar cell generated electricity.

Keywords: *Archimedes spiral wind turbine; small wind turbine; wind–solar hybrid; urban wind energy; power coefficient; Betz limit; 3D printing.*

1. INTRODUCTION

Most of the time, wind energy comes from large, lift-driven turbines that require strong, steady wind in an open area; unfortunately, many city rooftops do not provide the same conditions and typically experience slow, turbulent wind [1, 2]. Furthermore, small, lift-driven turbines do not start rotating until the wind reaches a fairly high speed [8], and hybrid wind–solar kits are generally costly and difficult to modify to fit a specific roof. The Archimedes spiral wind turbine (ASWT), based on the Archimedes screw, is a horizontal-axis turbine that is driven by both lift and drag [3] and has been shown to perform well at the low wind speeds and low tip speed ratios characteristic of urban wind [4, 5]. Slow-moving spiral rotors are also commonly proposed as a way to reduce the noise and bird impacts associated with

propeller-driven rotors [6]; however, this study did not measure either. In India, hybrid wind–solar systems fall within the policy and programme remit of the Ministry of New and Renewable Energy [7].

This research project compared the rotational speed, electrical power generation and power coefficient of four different small 3D-printed ASWT rotors. It also tested whether a unit built around one of these rotors could generate enough electricity to power light-emitting diodes (LEDs). The comparison was exploratory, with several variables changing at once, rather than a single-variable experiment, since all five design parameters (radius, mass, blade angle, length and wall thickness) varied among the four rotors (Table 1). After determining which rotor provided the most electrical output (Sample 1), a hybrid unit with a red LED and two solar cells was built around it. The prototype was built only to show whether it could provide enough electricity to light a few LEDs, and the rotors were tested with a hairdryer and in real outdoor wind rather than in a controlled wind tunnel (Section 6.6).

2. LITERATURE REVIEW

2.1 The urban wind resource

Compared to the open-field conditions that most commercial wind turbines are designed for, urban environments provide a lower average wind speed, higher turbulence levels and more variability in wind direction [1, 2]. A case study of Berlin by Wilke, Shen and Ritter [9] indicated that small-scale wind generation may be feasible, but that it will likely need to be combined with other sources of energy. Tsionas, Llaguno-Munitxa and Stephan [6] evaluated the environmental impacts of small-scale wind generation, such as noise and bird strike.

2.2 Optimising the aerodynamic performance of the Archimedes spiral rotor

Kim et al. [10] developed a numerical model based on experimental data to evaluate the power coefficient of the ASWT. They reported a power coefficient of approximately 0.25. Similarly, Jang et al. [11] simulated the performance of the ASWT with field-data validation and found that the maximum power coefficient was 0.293 at a tip speed ratio of 2.19. Wind-tunnel tests by Kamal et al. [12] showed that the maximum power coefficient (C_P) of a conventional rotor was 0.243 at a tip speed ratio of 1.5. However, an aerofoiled version achieved a C_P of 0.3045 at a tip speed ratio of 2.

Additionally, Refaie et al. [3] reported a maximum C_P of 0.311 for a rotor with a concentrator; however, this value was determined using numerical methods. Optimisation studies usually focus on a single parameter at a time. Examples of parameters that have been studied include blade angle [4], blade geometry and shape [12–14], winglets, which increased peak C_P by 13.4% [15], and shrouds [17]. One study [16] utilised a genetic algorithm to optimise all of the geometric features of the rotor, and Faisal et al. [5] reviewed several optimisation techniques. The Liam F1 [18] is currently available for residential applications; however, the manufacturer's performance claims have not undergone independent review. The theoretical background used in this research effort is consistent with Tong [19], and IEC 61400-2 [20] establishes design and safety standards for small wind turbines; however, this prototype does not claim to meet these requirements.

2.3 Scale effects in very small turbines

In general, as turbines decrease in size, their performance decreases. Blades that operate at low Reynolds numbers experience laminar separation, which causes a decrease in lift and an increase in drag [21]. Surface roughness does not scale with the rotor. Erosion and damage to the leading-edge surface can cause an increase in drag and a reduction in lift [22]; however, these measurements were taken at significantly higher Reynolds numbers. Additionally, FDM-printed PLA is rougher at larger layer thicknesses [23], and resistive torques caused by bearings, brushes and cogging become increasingly significant problems as turbines decrease in size [8, 24]. Centimetre-scale turbines generally produce microwatts to milliwatts of electrical power: a 2 cm shrouded rotor produced 0.08 to 2.5 mW at wind speeds ranging from 3 to 7 m/s [25], and Zakaria et al. [26] evaluated a centimetre-scale swirl-type turbine.

2.4 Research gap

Most studies of the performance and design of such rotors are conducted on larger rotors in wind tunnels, by means of computer simulation, or both. A 3D-printed ASWT has recently been optimised and evaluated as a generator of electricity [27]. The current study makes no claim to novelty in either the manufacture of a 3D-printed ASWT or the use of an ASWT with solar cells. The more modest claim of the current study is to provide a low-cost comparison of four small 3D-printed rotors driving a single generator under a constant electrical load, and thereby to illustrate the limitations of direct drive in terms of the maximum possible power output at this scale, based on the measured electrical characteristics of each rotor–generator combination.

3. THEORETICAL BASIS AND OPERATING PRINCIPLE

3.1 Principle of operation

The SpiralWatt turbine uses three helically shaped blades mounted on a horizontal axis. The axis of rotation of the turbine was parallel to the airflow when tested with a hairdryer, as is typical for Archimedes spiral wind turbines [10, 11]. During testing outside, the turbine head was rotated manually around its vertical support to align with the changing wind direction; however, the wind direction continued to change throughout each test. When air passes through the turbine rotor, it follows the helix. Therefore, each blade experiences a pressure differential (lift) on one side and a resistive force (drag) on the opposite side, resulting in a net torque applied to the turbine shaft. There is no yaw system to allow the rotor to orient itself towards the wind.

3.2 Power, power coefficient and tip speed ratio

The power available in the wind that flows over the swept area of the turbine rotor and the mechanical power developed by the turbine rotor are calculated using Equations (1) and (2) respectively. The variables used in these calculations are air density (ρ), swept area (A), turbine rotor radius (r), wind velocity (v) and aerodynamic power coefficient (C_P):

$$P_{wind} = \tfrac{1}{2} \rho A v^3, \quad A = \pi r^2 \tag{1}$$

$$P_{mech} = C_P P_{wind} \quad (2)$$

Torque on the shaft was not determined; therefore, the aerodynamic power coefficient could not be calculated directly. Instead, the electrical power produced by the turbine (Equation 3) was used to determine the electrical power coefficient, $C_{P,e}$ (Equation 4). The value of $C_{P,e}$ considers both the efficiency of the generator (η_{gen}) and the electrical losses (η_e):

$$P_{elec} = V I \quad (3)$$

$$C_{P,e} = P_{elec} / P_{wind} = C_P \eta_{gen} \eta_e \quad (4)$$

As stated above, $C_{P,e}$ will always be less than C_P; however, due to uncertainty in determining the wind power (Section 3.6), $C_{P,e}$ cannot be considered a lower bound. The tip speed ratio (TSR), λ, is determined from either the angular velocity ω or the rotational speed N of the turbine rotor in revolutions per minute (rpm):

$$\lambda = \omega r / v = 2\pi N r / (60\ v) \quad (5)$$

An additional coefficient, $C_{P,e,jet}$, can be defined as the ratio of the electrical power produced by the turbine to the jet reference power. The jet reference power is based on the area covered by the 8.2 cm outlet (outer diameter d_n) of the hairdryer. This area is smaller than any of the turbine rotors:

$$P_{jet} = \tfrac{1}{2} \rho A_{jet} v^3, \quad A_{jet} = \pi d_n^2 / 4 = 5.28 \times 10^{-3}\ m^2 \quad (6)$$

This assumes that the entire outlet area is filled with a uniform jet travelling at a single speed. A free jet, however, expands after exiting the outlet and has a non-uniform velocity profile [28]. Since the jet speed was only measured at one point, $C_{P,e,jet}$ is a reference value, not an actual measurement of efficiency, and it is not compared with published power coefficients or with the Betz limit.

3.3 Theoretical limit: Betz limit, not drag limit

The Betz limit is developed by applying the principles of mass and momentum conservation to an idealised actuator disc. The Betz limit represents a maximum power coefficient of 16/27 (approximately 0.593) and applies to all types of rotating devices in free-flowing air, regardless of the forces exerted on the blades, as long as the power coefficient is calculated based on the swept area [19]. A flat plate blown downwind will produce a power output that can be expressed as $P = \tfrac{1}{2}\rho A C_D (v - u)^2 u$, where u is the velocity of the flat plate and C_D is the drag coefficient of the flat plate. The maximum power output occurs at $u = v/3$. When this occurs, the maximum power coefficient produced is 4/27 times the drag coefficient of the flat plate. If the drag coefficient of the flat plate is approximately equal to 1, then the maximum power coefficient is approximately 0.148. Thus, this type of device cannot produce a tip speed ratio that is much larger than 1.

Reports from the literature show that power coefficients for ASWTs range from 0.243 to 0.311 [3, 10–12]. Reports from the literature also indicate that optimal tip speed ratios for ASWTs are between 1.5 and 2.2 [3, 11, 12]. As reported in the literature, the power coefficients for ASWTs are considerably higher than predicted by the drag model.

Furthermore, aerofoil blades and winglets, which increase the lift-to-drag ratio and decrease the formation of tip vortices, considerably increased the power coefficient for ASWTs by 26.88% [12] and 13.4% [15].

Refaie et al. [3] categorise the ASWT as a lift–drag turbine. In contrast, Jang et al. [11] describe the ASWT as a drag-type turbine, although they reported a power coefficient of 0.293.

This study treats the ASWT as a lift–drag turbine and considers the Betz limit as the theoretical maximum possible power coefficient for the ASWT. Unfortunately, the data from SpiralWatt do not contain sufficient information to determine whether the ASWT operates primarily as a lift-producing turbine or as a drag-producing turbine. The fact that the tip speed ratios of Samples 2 to 4 were all greater than 1 (see Section 6.4) supports the possibility that some amount of lift may have been generated by these turbines; however, it is also possible that a considerable amount of drag was generated by these turbines.

3.4 Air density

The hairdryer was used on its cold setting. Air density depends on temperature T and pressure p through the ideal gas law, with $R_d = 287.05$ J/(kg·K):

$$\rho = p / (R_d T) \tag{7}$$

Neither was recorded, so the sea-level value of 1.225 kg/m^3 was used. At New Delhi's elevation (about 220 m, about 98.8 kPa) and 30 °C, Equation (7) gives 1.14 kg/m^3, so the wind power may be overestimated, and $C_{P,e}$ underestimated, by up to about 7%, which is small compared with the anemometer uncertainty.

3.5 Generator behaviour

The generator is a permanent-magnet DC motor coupled directly to the rotor. Its internal voltage is proportional to its speed, and its current depends on the load:

$$V = k_e \omega - I R_{int}, \quad I = V / R_L \tag{8}$$

Here, I is the current, V the terminal voltage, k_e the back-EMF constant, and R_{int} and R_L the winding and load resistances; the torque is proportional to the current, with the same constant [29]. For the fixed benchmark load, Equation (8) gives $P_{elec} = (k_e\omega)^2 R_L / (R_L + R_{int})^2$, so the electrical power is proportional to the square of the generator speed. At a fixed speed, the most power goes to the load when $R_L = R_{int}$.

The 29.2 Ω load used here is about 10 times the winding resistance (Section 4.2), so about 91% of the generator's internal electrical power reaches the load. A lower load would draw more power at a given speed but also brake the rotor more, so the best load would have to be found experimentally. Adding the winding voltage drop to the terminal voltage gives the internal voltage, whose ratio to speed should be constant for one generator; this is used to check the data in Section 6.1.

3.6 Measurement uncertainty

Assuming independent inputs, the relative uncertainty in $C_{P,e}$ follows from Equations (1), (3) and (4), where δ is the uncertainty in each quantity:

$$(\delta C_{P,e}/C_{P,e})^2 = (\delta V/V)^2 + (\delta I/I)^2 + (3\delta v/v)^2 + (2\delta r/r)^2 + (\delta\rho/\rho)^2 \tag{9}$$

The wind-speed term dominates because the wind speed is cubed; for $C_{P,e,jet}$, the radius term is replaced by the outlet-diameter term. The budget excludes run-to-run variation, flow non-uniformity and the air-density error, so it is a lower bound.

4. MATERIALS AND METHODS

4.1 Rotor samples

The four rotors were designed with CAD and then printed vertically using a 0.4 mm nozzle with Bambu Lab PLA Lite. A 0.2 mm layer height was used, along with five wall loops and 10% infill (Figure 1). All four rotors have three blades and four helical turns. They were numbered in ascending order based on their radii. After printing, no finishing was done on them; therefore, the balance of each rotor depends solely on the symmetry of its shape. The blade angles listed in Table 1 are the design (CAD) angles, which were taken from the axis of rotation of the shaft at the base of the blade. Each rotor was press-fitted onto the generator's shaft. Since the rotors differ not only in size (radius) and weight (mass) but also in the angle of the blade, the length of the blade and the thickness of the blade walls, it is impossible to isolate the effect of any one variable.

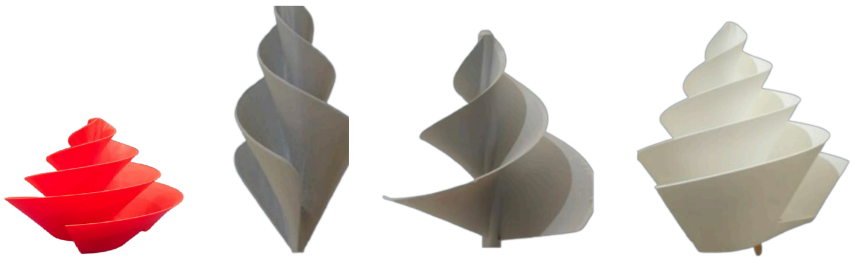


Figure 1. The four 3D-printed rotor samples (photographs not to scale). From left: Sample 1 (r = 5 cm, m = 30 g), Sample 2 (r = 10 cm, m = 100 g), Sample 3 (r = 13 cm, m = 150 g), Sample 4 (r = 14 cm, m = 200 g).

Table 1. Geometry of the four rotor samples (print settings are given in Section 4.1).

Parameter	**Sample 1**	**Sample 2**	**Sample 3**	**Sample 4**
Radius r (cm)	5	10	13	14
Swept area A (m^2)	0.0079	0.0314	0.0531	0.0616
Mass m (g)	30	100	150	200
Blade angle from shaft axis, at root (°)	38	43	51	41
Rotor length (cm)	15.2	22.3	18.1	18.4
Hub / shaft diameter (mm)	32	31	32	32
Blade wall thickness (mm)	1.2	1.4	1.1	1.7

4.2 Generator and electrical load

A REES52 RK027 5 V mini DC dynamo motor, a brushed permanent-magnet motor without a gearbox, was used as the generator for each of the four rotors. Multimeter 1 was set to the 200 Ω range (0.1 Ω resolution) and used to measure the winding resistance at five different shaft positions; the readings varied from 3.0 to 3.1 Ω, giving a mean value of approximately 3.0 Ω. There is no record of the meter lead resistance being measured or subtracted from the measured values.

The benchmark tests were carried out using the generator connected to a fixed resistor (nominal value 30 Ω, measured value 29.2 Ω) whose current depends solely on the voltage across it. Unlike diodes or capacitors, a resistor does not exhibit threshold or stored-charge effects. It should be noted that this resistor was not chosen based on maximum power transfer considerations (see Sections 3.5 and 6.6). A voltmeter was connected across the resistor and an ammeter was connected in series with it; both instruments measured time-averaged DC voltages and currents, to 0.01 V and 0.1 mA respectively. The electrical power was then calculated as $P_{elec} = VI$. The average V/I ratio over 48 readings was 30.1 ± 0.8 Ω, which is within 3% of the measured resistance; therefore, the two meters agree with each other.

4.3 Hybrid unit and circuit components

Table 2 provides a list of the components required to construct the hybrid unit. Figures 2 and 3 illustrate the circuit diagram and photographs of the assembled unit respectively. Both the generator and the two series-connected solar cells individually supply a common node via each source's own 1N5819 Schottky diode. The purpose of these diodes is to prevent reverse currents from flowing between the sources and to provide low voltage drops compared with silicon diodes. The red LED is supplied by the common node through a 100 Ω resistor. Data derived from an earlier version of the same design, in which the solar cells were directly connected across the generator, are not included here.

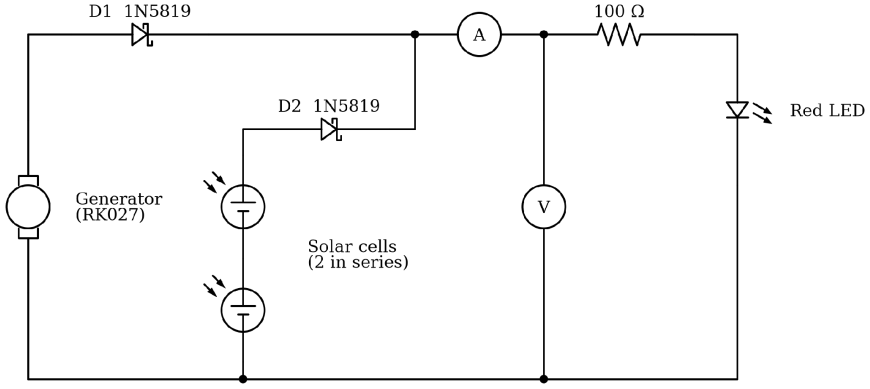


Figure 2. Circuit of the hybrid unit. The generator and the two series-connected solar cells each feed the common node through their own 1N5819 Schottky diode; the ammeter (A) is where the two diodes join, and the voltmeter (V) is across the LED branch (100 Ω resistor and red LED).

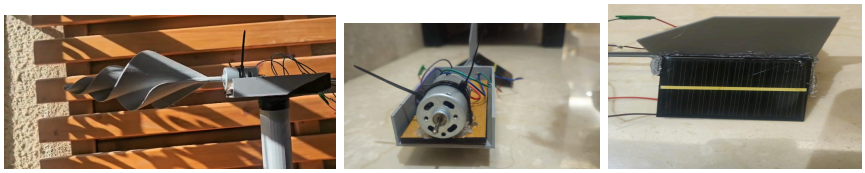


Figure 3. The hybrid unit. (a) The assembled unit outdoors on its mast, shown here fitted with the Sample 3 rotor turning in the wind (frame from a video); the hybrid measurements in Table 5 were made with Sample 1. (b) One of the two monocrystalline solar cells (60 × 60 mm) mounted on an adjustable 3D-printed fin. (c) The RK027 generator in its 3D-printed housing, shown with the rotor removed; the rotor is press-fitted onto the exposed shaft.

Table 2. Components of the hybrid unit.

Component	Specification / rating	Qty	Purpose
Rotor	Sample 1 (Table 1)	1	Converts wind to shaft rotation
DC generator	REES52 RK027 5 V DC motor, direct drive	1	Converts shaft rotation to electricity
Blocking diodes	1N5819 Schottky, one per source	2	Isolate the two sources
LED	Red indicator LED with a 100 Ω series resistor	1	Load and visual indicator
Digital multimeters	See Table 3	2	Voltage and current measurement
Solar cells	Monocrystalline, 60 × 60 mm, 5 V and 0.44 W each; in series (0.88 W total)	2	Solar input; mounted at 45°
Frame and bearings	3D-printed PLA frame; lubricated bearings	1 set	Supports and aligns the shaft
Fins	Adjustable 3D-printed fins	as needed	Hold the solar cells

4.4 Instrumentation

The instruments are listed in Table 3. The anemometer was held in the jet about 5 cm upstream of the rotor face, in the same position for every test. The hairdryer (Dyson Supersonic Nural, 1380 W) was used on its cold setting without attachments; its outlet is a ring of 7.9 to 8.2 cm outer diameter, and 8.2 cm was used for the outlet area.

Table 3. Measuring instruments.

Instrument	Make / model	Quantity measured	Resolution	Stated accuracy
Vane anemometer	UNI-T UT363 (0–30 $m \cdot s^{-1}$)	Wind speed v	0.1 $m \cdot s^{-1}$	±(5% of reading + 0.5 $m \cdot s^{-1}$)
Digital multimeter 1	Duratool D03124 (2000-count)	Voltage V (DC, 2 V and 20 V ranges)	0.001 V / 0.01 V	±(0.5% of reading + 2 counts)
Digital multimeter 2	Duratool D03124 (2000-count)	Current I (DC, 200 mA range)	0.1 mA	±(1.5% of reading + 3 counts)
Laser tachometer	UNI-T UT373 (non-contact)	Rotational speed N	0.1 rpm	±(0.04% of reading + 2 digits)
Digital scale	StealODeal SF-400A (0–7 kg)	Rotor mass m	1 g	Not stated
Digital caliper	Generic MDIGI6, 0–150 mm	Radius r, other dimensions	0.01 mm	Not stated

4.5 Test procedure

Benchmark tests. In still air, each rotor was tested first (control). Then, using a hairdryer positioned directly along the axis of each rotor, 25 cm from the front of the rotor, the rotor was tested at each of its three speeds (low, medium and high). Finally, each rotor was tested under natural wind conditions. After the rotor reached steady-state operation, the wind speed, rotational speed (using a UNI-T UT373 laser tachometer), voltage and current were measured consecutively. Each trial was repeated three times, and each time the rotor was allowed to stop spinning before the trial was repeated. The mean values are shown in Table 4, and the individual data points are included in the raw data log that accompanies this revision and are available on request. All trials were conducted in New Delhi on 5 October 2026. The trials conducted in natural wind began at around 09:30.

Operating wind speed. Since the wind speeds were not varied in a controlled manner, it is impossible to determine the cut-in speeds for each rotor (see Section 5.2).

Hybrid tests. Sample 1 was tested in the hybrid system outdoors on 5 October 2026 at 3:40 pm. Three separate trials were conducted: solar cells alone (rotor stationary), turbine alone (cells disconnected), and both solar cells and turbine. Measurements taken during these trials included wind speed, rotational speed, and voltage and current in the LED branch (measured to within 0.1 V and 1 mA). The ammeter was placed at the intersection of the two diodes. Whether or not the LED lit up was also noted. Trial runs used to verify the wiring are excluded from this report. Solar irradiance was not measured.

4.6 Measured and calculated values

All values, including wind speed, rotational speed, voltage, current, radius and mass, were measured directly. Values such as P_{elec}, P_{wind}, P_{jet}, $C_{P,e}$, $C_{P,e,jet}$ and λ were calculated from Equations (1)–(6). An air density of 1.225 kg/m^3 was assumed for all calculations. No values were calculated based on assumed

efficiencies or tip speed ratios. The uncertainty in $C_{P,e}$ calculated from Equation (9) ranged from 27% to 45%. This uncertainty was primarily due to the anemometer (5% of reading plus 0.5 m/s, or 9% to 15% in wind speed), and the voltage and current terms contributed less than 3% and 5% respectively. $C_{P,e,jet}$ had an additional 12% uncertainty from an assumed 0.5 cm uncertainty in the jet diameter. Run-to-run variation was represented as the standard deviation of the three repeat trials.

5. RESULTS

5.1 Benchmark tests

Table 4. Benchmark results for the four rotors with the fixed 29.2 Ω load, numbered in order of increasing radius (means of three readings; P_{elec} as mean ± one standard deviation).

Condition	**v ($m \cdot s^{-1}$)**	**N (rpm)**	**V (V)**	**I (mA)**	**P_{elec} (mW)**	**P_{wind} (W)**	**$C_{P,e}$ (disc)**	**$C_{P,e,jet}$**	**λ**
Sample 1 (r = 5 cm, m = 30 g)									
Outdoor	5.0	1117	0.66	22.2	14.8 ± 1.5	0.61	0.0240	—	1.16
Hairdryer – Low	6.5	1507	0.98	32.7	31.9 ± 0.7	1.32	0.0241	0.0359	1.21
Hairdryer – Medium	9.1	2039	1.16	37.7	43.6 ± 3.1	3.63	0.0120	0.0179	1.17
Hairdryer – High	12.3	2685	1.48	47.7	70.4 ± 2.7	8.95	0.0079	0.0117	1.14
Sample 2 (r = 10 cm, m = 100 g)									
Outdoor	5.2	783	0.49	16.4	8.1 ± 0.9	2.76	0.0029	—	1.57
Hairdryer – Low	6.5	1014	0.63	21.2	13.4 ± 1.3	5.37	0.0025	0.0148	1.62
Hairdryer – Medium	9.0	1425	0.82	27.0	22.2 ± 0.9	14.18	0.0016	0.0093	1.65
Hairdryer – High	12.6	1829	1.09	35.6	39.0 ± 3.2	38.80	0.0010	0.0060	1.52
Sample 3 (r = 13 cm, m = 150 g)									
Outdoor	5.2	572	0.34	11.1	3.8 ± 0.3	4.66	0.00082	—	1.49

Condition	v ($m \cdot s^{-1}$)	N (rpm)	V (V)	I (mA)	P_{elec} (mW)	P_{wind} (W)	$C_{P,e}$ (disc)	$C_{P,e,jet}$	λ
Hairdryer – Low	6.7	742	0.43	14.2	6.1 ± 0.4	9.64	0.00064	0.0064	1.52
Hairdryer – Medium	9.2	1162	0.69	22.9	15.8 ± 1.0	25.60	0.00062	0.0062	1.71
Hairdryer – High	12.6	1510	0.87	29.6	25.8 ± 2.2	65.57	0.00039	0.0040	1.63
Sample 4 (r = 14 cm, m = 200 g)									
Outdoor	5.6	574	0.33	11.0	3.6 ± 0.2	6.51	0.00055	—	1.51
Hairdryer – Low	6.7	707	0.40	13.2	5.3 ± 0.6	11.34	0.00046	0.0054	1.55
Hairdryer – Medium	9.4	972	0.57	19.4	11.1 ± 0.4	30.99	0.00036	0.0042	1.52
Hairdryer – High	12.4	1300	0.73	24.9	18.3 ± 0.9	72.49	0.00025	0.0029	1.53

Notes: P_{wind} is calculated over the full swept disc and P_{jet} over the area enclosed by the 8.2 cm hairdryer outlet ($A_{jet} = 5.28 \times 10^{-3}$ m^2), both with $\rho = 1.225$ $kg \cdot m^{-3}$ and the mean wind speed; $C_{P,e}$ (disc) = P_{elec} / P_{wind} and $C_{P,e,jet} = P_{elec} / P_{jet}$, given for hairdryer runs only; λ uses the mean rotational and wind speeds. In the indoor still-air control no rotor turned, so those runs are not shown. The individual readings are included in the raw measurement log supplied with this revision and are available on request.

Electrical power increased with wind speed for every rotor (Figure 4). At the highest hairdryer setting (12.3–12.6 m/s), Samples 1 to 4 generated 70.4, 39.0, 25.8 and 18.3 mW respectively, and outdoors (5.0–5.6 m/s) they generated 14.8, 8.1, 3.8 and 3.6 mW. In both conditions, each successively larger design produced less power, and the largest rotor produced the least. The standard deviation of the repeated trials was 2% to 12% of the mean power.

At the highest setting, rotational speed decreased from 2685 rpm for Sample 1 to 1300 rpm for Sample 4, and voltage and current decreased in a similar way (1.48 V and 47.7 mA for Sample 1 against 0.73 V and 24.9 mA for Sample 4). From the lowest to the highest setting, output increased by a factor of 2.2 to 4.2 while v^3 increased by a factor of approximately 6.3 to 7.3, so the power coefficient decreased as wind speed increased.

$C_{P,e,jet}$ ranged from 0.0029 to 0.036 and decreased with increasing wind speed for each rotor (Figure 5b). Outdoors, the $C_{P,e}$ values based on the rotor disc area were 0.024, 0.0029, 0.0008 and 0.0006 for Samples 1 to 4 (Figure 5a). Tip speed ratios remained relatively constant as wind speed changed: 1.14 to 1.21 for Sample 1 and 1.49 to 1.71 for Samples 2 to 4.

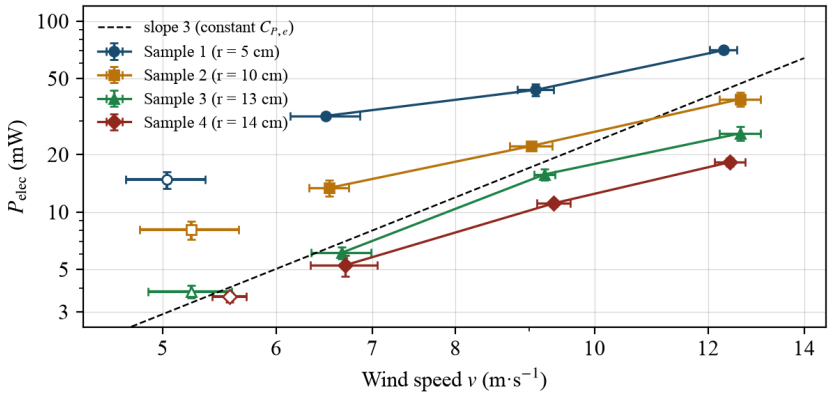


Figure 4. Electrical output against wind speed (log–log axes) with the 29.2 Ω load. Filled markers joined by lines are hairdryer runs and open markers are outdoor runs; error bars show one standard deviation of the three repeats. The dashed line shows the slope of 3 expected if $C_{P,e}$ were constant.

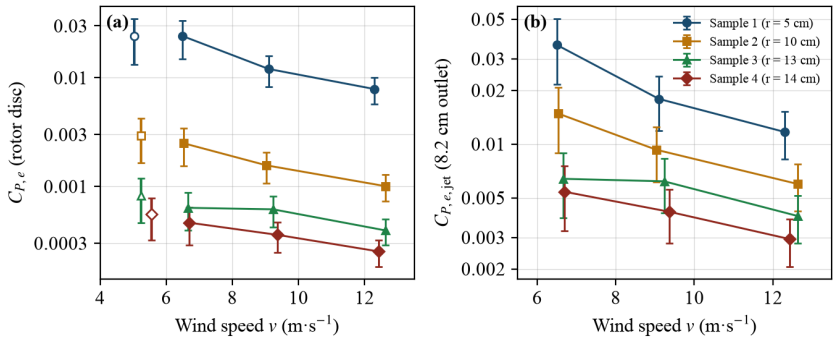


Figure 5. (a) $C_{P,e}$ referred to the rotor disc (open markers: outdoor runs); (b) $C_{P,e,jet}$ referred to the 8.2 cm outlet, hairdryer runs only. Error bars show instrument-propagated uncertainty only, from Equation (9) (±27% to ±45% in (a); ±30% to ±40% in (b)); they exclude flow-field effects and the air-density bias.

5.2 Lowest operating wind speeds

No rotor turned in still air. With the load attached, all rotors turned at the lowest outdoor wind speeds measured (4.8, 4.9, 4.9 and 5.4 m/s for Samples 1 to 4); these are not cut-in speeds.

5.3 Hybrid unit

The hybrid results for Sample 1 are given in Table 5.

Table 5. Hybrid unit results with the Sample 1 rotor (P_{elec} delivered to the LED branch; P_{wind} calculated with $\rho = 1.225\ kg \cdot m^{-3}$).

Condition	**v ($m \cdot s^{-1}$)**	**N (rpm)**	**V (V)**	**I (A)**	**P_{elec} (W)**	**P_{wind} (W)**	**$C_{P,e}$**	**λ**
Solar cells only, outdoors (rotor stopped)	—	0	4.6	0.023	0.106	—	—	—
Turbine only, outdoors (solar cells disconnected)	5.5	1168	0.73	0 displayed (< 0.001 A)	≈0	0.80	≈0	1.11
Solar cells and turbine, outdoors	5.7	1183	4.8	0.027	0.130	0.89	not defined (combined output)	1.09

In an outdoor experiment using the solar cell array alone as the power source for the LED branch, the solar cell array provided 4.6 V and consumed 23 mA (0.106 W) and illuminated the LED. The wind turbine alone (1168 rpm and 5.5 m/s wind speed) was providing 0.73 V to the LED branch, there was no measurable current at the 1 mA recording resolution and the LED was not illuminated. Simultaneous operation of both devices (1183 rpm and 5.7 m/s wind speed) provided 4.8 V to the LED branch and consumed 27 mA (0.130 W) and illuminated the LED. The LED experienced a voltage drop of 2.1–2.3 V in all cases where it was illuminated. For an LED to conduct electricity, it needs a minimum threshold voltage. Typically, this voltage for a red LED is between 1.8–2.0 V [30]. The two solar cells connected in series were able to supply more than this.

Although rated at 5 V each, they only delivered 4.6–4.8 V to the common node. One reason for this might be that the low current produced by the solar cells under the limited amount of available sunlight allowed the LED branch to establish the voltage across itself. The 0.106–0.130 W generated by the solar cell pair represents about 12–15% of their total rated capacity of 0.88 W, and appears reasonable since the load was not matched to the cells. The maximum internal voltage created by the wind turbine during the outdoor testing was roughly 0.75 V, and the highest voltage created by the wind turbine in any test was 1.52 V. Both of these voltages are too low for the LED to be illuminated.

6. DISCUSSION

6.1 Rotational speed, voltage and current

The sum of the voltage drop due to the winding resistance (IR_{int}, with $R_{int} \approx 3.0\ \Omega$) and the measured voltage gives the generator's internal voltage. Dividing this value by the rotational speed gives approximately 0.65 ± 0.04 mV per rpm (range 0.59–0.72) for all four samples, as one might expect for a single generator. These results correspond to $k_e \approx 0.0062$ V·s/rad. Since the winding resistance is only about 10% of the total load, it is unlikely to significantly influence this estimate. The turbine-only hybrid measurement provided an approximate additional consistency check. In this test, 0.73 V was recorded at 1168 rpm with no measurable current. Because this voltage was measured downstream of the blocking diode rather than directly across the generator terminals, it should not be interpreted as a precise open-circuit back-EMF measurement. This value is slightly less than the previous estimate. One possible reason for this discrepancy is a small voltage drop across the diode. The electromagnetic torque k_eI was estimated to range from 0.07 to 0.30 mN·m, with 0.30 mN·m for Sample 1 and 0.15 mN·m for Sample 4, both at the high setting [29].

When operating with a constant load, the power generated varies with the square of the speed (Section 3.5). Furthermore, when operating at a constant wind speed and tip speed ratio, smaller rotors will turn faster than larger ones (Equation 5). It appears that much of the variation in the rankings can be accounted for by this relationship: at the high setting, the ratio of the power generated by Samples 1 and 4 (3.9) is very close to the ratio of the squares of their speeds (4.3). Outdoors, the corresponding values were 4.1 and 3.8 respectively. Larger rotors may provide more aerodynamic torque than smaller ones; however, shaft torque was not measured. At their lower speeds, the generator voltage is too low to create a significant current. Therefore, very little of that torque will be converted into usable electrical energy. Under the hairdryer tests, increasing rotor diameter did not necessarily expose the rotor to proportionally greater incident wind power because the nominal outlet was smaller than every rotor and the downstream jet profile was not measured.

The mismatch between the speeds of the rotors and the generator represents a major limitation of the prototype; however, without measurement of the torque, it is impossible to separate the effect of this mismatch from aerodynamic effects, frictional losses within the system or limitations in the efficiency of the generator. Larger rotors would need to use either step-up gears or a low-speed generator to exploit their size. The calculated tip-speed ratios remained relatively stable with changing wind speed for each rotor. However, because the hairdryer jet was narrower than every rotor and its velocity profile was not measured, these TSR values should be interpreted as reference values based on the measured centreline wind speed rather than precise whole-rotor aerodynamic tip-speed ratios..

Recording voltages to within 0.01 V introduces a potential source of error of up to 1.6% at the lower end of the readings. Additionally, for Sample 1 at the medium setting, the rotational speed varied by 14% between successive trials, while the voltage varied by only 6%. While both variables should exhibit similar variability, it is conceivable that the rotor slipped on its shaft, or that the readings were recorded at slightly different intervals.

6.2 Power coefficients in context

The outdoor disc-based $C_{P,e}$ values (0.0006–0.024) were one to three orders of magnitude lower than the published aerodynamic C_P values for optimised ASWTs (0.24–0.31) [3, 12]. Some of this difference can be explained by the fact that the generator, friction and electrical loss terms are included in the $C_{P,e}$ calculation (Equation 4). When considering overall power generation, however, the values obtained in this study were consistent with other centimetre-scale turbines that generate between microwatts and milliwatts [25, 26].

The ranking remains unaffected regardless of whether the rotor disc area or the outlet area is used as the reference. At all settings, Sample 1 had a higher power coefficient ($C_{P,e}$) than the other samples. Using the disc area as the reference penalises the larger rotors under the hairdryer. The outlet diameter of 8.2 cm is smaller than all rotor diameters (10, 20, 26 and 28 cm). The disc area is 1.5 times the outlet area for Sample 1, while it is 5.9–11.7 times for Samples 2 to 4. If the outlet area is used as the reference, Sample 1 continues to have the highest power coefficient at every setting (0.012–0.036 compared with 0.0029–0.015). Due to the lack of measurement of the velocity profile of the jet, neither method provides an exact measure of the power delivered to the blades.

However, the rankings are identical for both methods and in the field. Outdoors, the disc-based values may be more relevant, but estimating the effective area is challenging due to varying wind directions. All outdoor values represent averages of three readings taken during gusty conditions, with approximately 45% instrument uncertainty. Notwithstanding this uncertainty, Sample 1's value of 0.024 represents an 8–44-fold increase over the values for the larger rotors.

6.3 Explanation for the low power coefficient at this scale

Several factors identified in previous studies may contribute to the low $C_{P,e}$ at this scale. None of these factors is specific to the spiral shape, and none was quantified individually in this study.

First, the rotor-scale Reynolds number vr/ν ($\nu \approx 1.5 \times 10^{-5}$ m^2/s) ranged from approximately 1.7×10^4 to 1.2×10^5. These values are one to two orders of magnitude below those of full-scale turbines and probably lie within the range where laminar separation limits blade efficiency [21].

Second, the printed layer lines make the blade surfaces rough, particularly at greater layer heights [23]. This roughness does not decrease with rotor size, and roughness increases drag and decreases lift on aerofoils [22], although its effect at low Reynolds numbers is less well understood [21].

Third, bearing and brush friction and cogging are relatively independent of wind speed, whereas aerodynamic torque increases roughly as r^3; therefore, resistive torque is a larger proportion of the available torque for smaller rotors [8, 24]. Even small amounts of friction matter when the electromagnetic torque is only 0.07 to 0.30 mN·m. Fourth, the RK027 is a small brushed DC motor used here as a generator; at the low voltages and powers produced in this experiment, brush contact, bearing friction and core losses may represent a substantial fraction of the available shaft power [29]; winding losses were only about 9%. Fifth, all four rotors were tested with the same load (29.2 Ω) and with a narrow, uneven hairdryer jet.

Therefore, these results provide limited information about ASWT aerodynamics, for which previously published studies [3, 10–12] are a better reference; this paper serves as a baseline study for this prototype.

6.4 Tip speed ratio

The published optimal tip speed ratios for ASWTs range from 1.5 to 2.2 [3, 11, 12]. The published optimal tip speed ratios for propeller turbines are 5 to 7 [19]. The tip speed ratio of Sample 1 ranged from 1.14 to 1.21. The tip speed ratio of Samples 2 to 4 ranged from 1.49 to 1.71. Sample 1 also produced the highest current and electromagnetic torque. At the same time, Sample 1 had the lowest tip speed ratio. This is consistent with Sample 1 being braked the most by the electrical load (see Section 6.1). Even if the highest possible value in the wind speed uncertainty range is used, Samples 2 to 4 will still have a tip speed ratio of approximately 1.3 or greater. This is consistent with a portion of the total force on the blades being due to lift. However, since the tip speed ratio measures only motion, it cannot show which forces are acting on the blades (see Section 3.3). If the same calculation is performed for Sample 1, the result is approximately 1.0. Thus, there is no evidence that the tip speed ratio is greater than 1 for this particular rotor. The outdoor tests provided an independent comparison without the restricted hairdryer jet; however, because they were conducted on a balcony, nearby building surfaces may have produced turbulence, recirculation and spatial variations in wind speed and direction. The similar outdoor TSR values for Samples 2–4 (1.57, 1.49 and 1.51) therefore support, but do not prove, that these rotors operated in a similar kinematic regime.

6.5 Hybrid unit

The hybrid unit provided power to the LED branch via the solar cells' own diode. The wind turbine, however, did not provide any power (see Section 5.3). It is likely that the slightly greater power and current with both sources, compared with the solar cells alone, is due to variation in solar irradiance between the consecutive measurements, rather than to an additional power contribution from the wind turbine. The voltage produced internally by the wind turbine is very low (around 0.75 V); therefore, it cannot produce enough voltage to drive current through its own diode. For the wind turbine to deliver appreciable current to the common node, its voltage would need to exceed the approximately 4.8 V common-node voltage by at least the forward voltage required by its Schottky diode. To get the wind turbine to generate more voltage, either a step-up gearbox or a DC–DC boost converter could be used. Both options require an appropriate match to the input of the wind turbine to avoid causing the rotor to stall. By doing this, the wind turbine may then contribute to the total amount of power generated by the hybrid system. Therefore, the findings of this research indicate that the two sources (the solar cells and the wind turbine) can operate independently of each other. However, the findings do not demonstrate that the two sources can work together to produce power.

6.6 Limitations

The first limitation of the study is that the hairdryer jet had a much smaller diameter than all of the rotors. The second limitation is that the velocity profile of the hairdryer jet was never determined; therefore, neither the coefficient based on the rotor disc area ($C_{P,e}$) nor the coefficient based on the area of the hairdryer outlet ($C_{P,e,jet}$) accurately represents the amount of energy provided to the rotor. The third

limitation of the study is that the wind speed was determined by taking a measurement at one location, which results in a potential error in $C_{P,e}$ ranging from 27% to 45% due to the anemometer alone. The fourth limitation of the study is that air temperature and pressure were not measured, and there were no facilities for testing in a wind tunnel.

Additionally, shaft torque was not measured in this study. This made it impossible to separate the contribution of C_P from the losses in the generator and other electrical components. Only one load (approximately ten times the winding resistance) was applied during this study, making it impossible to determine the maximum power point for each rotor. Voltage was only recorded to 0.01 V. As stated previously, the speed–voltage difference for Sample 1 at the medium setting still cannot be explained. Since the design variations were so complex, and only one sample of each design was tested, it is impossible to identify either the impact of each design variable or the variation between samples. The conditions were only tested three times, and roughness, generator efficiency and lead resistance were not measured. Therefore, the explanations given in Section 6.3 remain unquantified.

The outdoor tests were conducted on a balcony rather than in open terrain. Nearby walls, railings and the building façade may have produced turbulence and spatial variations in wind speed and direction. Consequently, the outdoor TSR and $C_{P,e}$ values should be interpreted as measurements under disturbed urban wind conditions rather than as free-field aerodynamic performance

Hybrid testing was performed consecutively, but no irradiance data were collected, and the resolution of the hybrid testing was lower than that of the benchmark testing. Finally, the prototype was not designed according to IEC 61400-2 [20]. It did not have an automatic yaw system, and it was not evaluated for noise or impacts on local wildlife.

7. CONCLUSION AND FUTURE WORK

The objective of this study was to compare four different 3D-printed Archimedes spiral rotors. A combined wind–solar unit was developed using the smallest rotor (Sample 1) and tested for powering LED lighting. The most effective rotor (Sample 1) had the highest power output (up to 70.4 mW) and power coefficient on both reference areas. As the rotor radius, mass and blade shape were varied simultaneously, it was impossible to isolate the effect of rotor size on the results. All the $C_{P,e}$ values were extremely small (at most 0.024 outdoors on a disc basis), much smaller than those reported in the literature for optimised ASWTs. The results are consistent with the output of the direct-drive generator under a constant load increasing with the square of speed, indicating that the generator was improperly selected for the larger, slower rotors. One of the primary findings of this study is that selecting a generator that matches the rotor speed is critical; however, without torque data, it is impossible to separate the contribution of the generator–rotor mismatch from aerodynamic and frictional losses. Tip speed ratios were nearly constant throughout the range of wind speeds tested (approximately 1.15 for Sample 1 and 1.5–1.7 for the other three samples); however, these ratios do not provide insight into the forces exerted on the blades.

Furthermore, low Reynolds number, surface roughness, friction and generator losses may have contributed to the small $C_{P,e}$ values.

When using the hybrid unit, the solar cells supplied the necessary voltage for operating the LED. A circuit was designed to isolate the two power sources from one another. In the turbine-only test, 0.73 V was insufficient to operate the LED. When the solar cells were connected, the turbine's internal voltage of approximately 0.75 V was also well below the approximately 4.8 V common-node voltage, and thus its blocking diode prevented it from supplying power. Thus, the two sources did not provide power simultaneously, and the second objective was only partially achieved.

Future studies should address: optimising the relationship between the rotor and generator through either step-up gearing or a low-speed generator; redesigning the hybrid circuit to incorporate a boost converter, maximum power point tracking and properly sized power sources and loads; conducting tests at multiple load resistances with continuous data collection; obtaining open-circuit voltage measurements versus speed, along with shaft torque measurements; testing in a wind tunnel wider than the largest rotor; and obtaining measurements of blade roughness, testing blades with smoothed surfaces, varying radius and mass independently, and obtaining records of solar irradiance and long-term rooftop performance.

DATA AVAILABILITY STATEMENT

Mean values are reported in Table 4. The individual benchmark readings are included in the raw measurement log supplied with this revision and are available on request. The raw measurement log and the calculation spreadsheet used to produce Tables 4 and 5 and Figures 4 and 5 have been supplied to the editors with this revision and are available from the author on request.

ACKNOWLEDGEMENTS

This project was carried out independently by the author, without a supervisor or mentor.

FUNDING

This research received no external funding.

CONFLICT OF INTEREST

The author declares no conflict of interest.

REFERENCES

[1] T. Stathopoulos, H. Alrawashdeh, A. Al-Quraan, B. Blocken, A. Dilimulati, M. Paraschivoiu, and P. Pilay, “Urban wind energy: Some views on potential and challenges,” *J. Wind Eng. Ind. Aerodyn.*, vol. 179, pp. 146–157, 2018, doi: 10.1016/j.jweia.2018.05.018.

[2] D. Micallef and G. van Bussel, “A review of urban wind energy research: Aerodynamics and other challenges,” *Energies*, vol. 11, no. 9, art. 2204, 2018, doi: 10.3390/en11092204.

[3] A. G. Refaie, H. S. Abdel Hameed, M. A. A. Nawar, Y. A. Attai, and M. H. Mohamed, “Qualitative and quantitative assessments of an Archimedes spiral wind turbine performance augmented by a concentrator,” *Energy*, vol. 231, art. 121128, 2021, doi: 10.1016/j.energy.2021.121128.

[4] K. Song, H. Huan, and Y. Kang, "Aerodynamic performance and wake characteristics analysis of Archimedes spiral wind turbine rotors with different blade angle," *Energies*, vol. 16, no. 1, art. 385, 2023, doi: 10.3390/en16010385.

[5] A. E. Faisal, C. W. Lim, B. A. J. Al-Quraishi, G. Alkawsi, C. H. Tan, J. Milano, C. C. Phing, K. Al-Farhany, and S. K. Tiong, "Investigating the techniques used for improving the aerodynamic performance of Archimedes spiral wind turbines: A comprehensive review and future work avenues," *Results in Engineering*, vol. 25, art. 103992, 2025, doi: 10.1016/j.rineng.2025.103992.

[6] I. Tsionas, M. Llaguno-Munitxa, and A. Stephan, "Environmental effects of urban wind energy harvesting: a review," *Buildings & Cities*, vol. 6, no. 1, pp. 1–24, 2025, doi: 10.5334/bc.491.

[7] Ministry of New and Renewable Energy, Government of India, *Annual Report 2022–23*, New Delhi, 2023.

[8] A. K. Wright and D. H. Wood, "The starting and low wind speed behaviour of a small horizontal axis wind turbine," *J. Wind Eng. Ind. Aerodyn.*, vol. 92, no. 14–15, pp. 1265–1279, 2004, doi: 10.1016/j.jweia.2004.08.003.

[9] A. Wilke, Z. Shen, and M. Ritter, "How much can small-scale wind energy production contribute to energy supply in cities? A case study of Berlin," *Energies*, vol. 14, no. 17, art. 5523, 2021, doi: 10.3390/en14175523.

[10] K. C. Kim, H. S. Ji, Y. K. Kim, Q. Lu, J. H. Baek, and R. Mieremet, "Experimental and numerical study of the aerodynamic characteristics of an Archimedes spiral wind turbine blade," *Energies*, vol. 7, no. 12, pp. 7893–7914, 2014, doi: 10.3390/en7127893.

[11] H. Jang, D. Kim, Y. Hwang, I. Paek, S. Kim, and J. Baek, "Analysis of Archimedes spiral wind turbine performance by simulation and field test," *Energies*, vol. 12, no. 24, art. 4624, 2019, doi: 10.3390/en12244624.

[12] A. M. Kamal, M. A. A. Nawar, Y. A. Attai, and M. H. Mohamed, "Archimedes spiral wind turbine performance study using different aerofoiled blade profiles: Experimental and numerical analyses," *Energy*, vol. 262, pt. B, art. 125567, 2023, doi: 10.1016/j.energy.2022.125567.

[13] M. A. A. Nawar, H. S. Abdel Hameed, A. Ramadan, Y. A. Attai, and M. H. Mohamed, "Experimental and numerical investigations of the blade design effect on Archimedes spiral wind turbine performance," *Energy*, vol. 223, art. 120051, 2021, doi: 10.1016/j.energy.2021.120051.

[14] A. M. Kamal, M. A. A. Nawar, Y. A. Attai, and M. H. Mohamed, "Blade design effect on Archimedes spiral wind turbine performance: Experimental and numerical evaluations," *Energy*, vol. 250, art. 123892, 2022, doi: 10.1016/j.energy.2022.123892.

[15] K. Song, H.-T. Huan, L.-C. Wei, and C.-X. Liu, "Performance analysis of a modified Archimedes spiral wind turbine having winglet on blade," *Energy*, vol. 333, art. 137389, 2025, doi: 10.1016/j.energy.2025.137389.

[16] O. Salah Samiani and M. Boroushaki, "Optimal design of Archimedes wind turbine using genetic algorithm," *Energy*, vol. 314, art. 134157, 2025, doi: 10.1016/j.energy.2024.134157.

[17] A. G. Refaie, H. S. Abdel Hameed, M. A. A. Nawar, Y. A. Attai, and M. H. Mohamed, "Comparative investigation of the aerodynamic performance for several shrouded Archimedes spiral wind turbines," *Energy*, vol. 239, art. 122295, 2022, doi: 10.1016/j.energy.2021.122295.

[18] B. Coxworth, "Screwy-looking wind turbine makes little noise and a big claim," *New Atlas*, 27 May 2014. [Online]. Available: https://newatlas.com/the-archimedes-liam-f1-urban-wind-turbine/32263/ (accessed 5 Oct. 2026).

[19] W. Tong, ed., Wind Power Generation and Wind Turbine Design. Southampton, UK: WIT Press, 2010.

[20] International Electrotechnical Commission, *IEC 61400-2: Wind Turbines — Part 2: Small Wind Turbines*, 2013.

[21] P. B. S. Lissaman, "Low-Reynolds-number airfoils," *Annu. Rev. Fluid Mech.*, vol. 15, pp. 223–239, 1983, doi: 10.1146/annurev.fl.15.010183.001255.

[22] A. Sareen, C. A. Sapre, and M. S. Selig, "Effects of leading edge erosion on wind turbine blade performance," *Wind Energy*, vol. 17, no. 10, pp. 1531–1542, 2014, doi: 10.1002/we.1649.

[23] I. Buj-Corral, X. Sánchez-Casas, and C. J. Luis-Pérez, "Analysis of AM parameters on surface roughness obtained in PLA parts printed with FFF technology," *Polymers*, vol. 13, no. 14, art. 2384, 2021, doi: 10.3390/polym13142384.

[24] J. R. P. Vaz, D. H. Wood, D. Bhattacharjee, and E. F. Lins, "Drivetrain resistance and starting performance of a small wind turbine," *Renew. Energy*, vol. 117, pp. 509–519, 2018, doi: 10.1016/j.renene.2017.10.071.

[25] D. A. Howey, A. Bansal, and A. S. Holmes, "Design and performance of a centimetre-scale shrouded wind turbine for energy harvesting," *Smart Mater. Struct.*, vol. 20, no. 8, art. 085021, 2011, doi: 10.1088/0964-1726/20/8/085021.

[26] M. Y. Zakaria, D. A. Pereira, and M. R. Hajj, "Experimental investigation and performance modeling of centimeter-scale micro-wind turbine energy harvesters," *J. Wind Eng. Ind. Aerodyn.*, vol. 147, pp. 58–65, 2015, doi: 10.1016/j.jweia.2015.09.009.

[27] M. A. H. Akash, M. S. Hossain, M. M. Hossain, and M. N. Islam, "Design optimization and performance evaluation of a 3D-printed Archimedes spiral wind turbine for renewable energy generation in Bangladesh," *Energy Reports*, vol. 15, art. 109125, 2026, doi: 10.1016/j.egyr.2026.109125.

[28] S. B. Pope, *Turbulent Flows*. Cambridge, UK: Cambridge University Press, 2000, ch. 5.

[29] A. Hughes and B. Drury, *Electric Motors and Drives: Fundamentals, Types and Applications*, 5th ed. Oxford, UK: Newnes (Elsevier), 2019.

[30] E. F. Schubert, *Light-Emitting Diodes*, 2nd ed. Cambridge, UK: Cambridge University Press, 2006.